Control of Dye Aggregation and Electron Injection for Highly Efficient Porphyrin Sensitizers Adsorbed on Semiconductor Films with Varying Ratios of Coadsorbate

Hsueh-Pei Lu,[†] Chen-Yuan Tsai,[†] Wei-Nan Yen,[‡] Chou-Pou Hsieh,[‡] Cheng-Wei Lee,[†,‡] Chen-Yu Yeh,*,[‡] and Eric Wei-Guang Diau*,[†]

Department of Applied Chemistry and Institute of Molecular Science, National Chiao Tung University, Hsinchu 300, Taiwan, and Department of Chemistry, National Chung Hsing University, Taichung 402, Taiwan
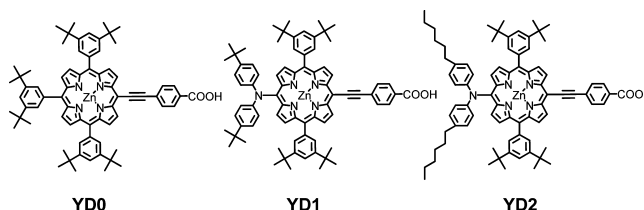
We report the photovoltaic performances and kinetics of femtosecond fluorescence for three zinc-porphyrin sensitizers (**YD0**−**YD2**) coadsorbed with chenodeoxycholic acid (CDCA) at three molar ratios on nanocrystalline semiconductor (TiO_2 or Al_2O_3) films. The addition of CDCA improved the efficiencies of **YD0** and **YD1** so that their maximum performance occurred at a dye/CDCA ratio of 1:2, but the presence of CDCA had a negative effect for **YD2**. Porphyrin aggregation on TiO_2 surfaces not only accelerates the rate of intermolecular energy transfer but also increases the rate of interfacial electron injection, so that the electron injection yields (Φ_{inj}) are balanced by these two important factors. As a result, Φ_{inj} increased slightly with increasing amount of CDCA for both **YD0** and **YD1**, but decreased for **YD2**; for this reason, the presence of CDCA failed to improve the photovoltaic performance for **YD2**, unlike for **YD0** and **YD1**. The cell performances were optimized on TiO_2 films of ∼10-μm thickness with a scattering layer of ∼4-μm thickness: the efficiencies of power conversion of **YD1** and **YD2** are slightly smaller than, but near, that of **N719**, being 6.5% and 6.8%, respectively, compared to 7.3%. Without a scattering layer on the films, the performance of **N719** was degraded significantly (6.3%), whereas the efficiencies of **YD1** and **YD2** decreased only slightly (6.4% and 6.6%), making this series of green sensitizers promising candidates for future light-penetrable photovoltaic applications.

1. Introduction

With advantages of low cost, low weight, coloring, and easy processing, dye-sensitized solar cells (DSSCs) are prospective alternatives for future devices for the conversion of solar energy, complementary to silicon-based solar cells.[1] DSSC devices with Ru complexes as photosensitizers have attained the greatest efficiency of power conversion, $\eta \approx 11\%$,[2] but a limited availability of Ru dyes and associated environmental concerns have stimulated much effort to find alternative, cheaper, and safer organic-based dyes.[3] Among those non-Ru-based dyes, porphyrin chromophores are promising candidates because they capture solar energy efficiently. Numerous reports of porphyrin-based DSSC have appeared.[3d,4] For example, a DSSC device with porphyrin sensitizers and a π-conjugated anchoring group functionalized at the β-position was reported to attain an efficiency of power conversion of $\eta = 7.1\%$,[4b] and a device made of a β,β'-edge-fused zinc porphyrin with quinoxaline moiety exhibited a comparable cell performance, $\eta = 6.3\%$.[3d] We reported a novel zinc porphyrin dye (**YD1**)[5] that has in its molecular structure an electron-donating diarylamino group attached at the meso position of the porphyrin ring opposite the meso-substituted phenylethynyl carboxyl anchoring group; a device made from this **YD1** dye was found to have a cell performance similar to that of a Ru-based DSSC, making the push−pull porphyrin the most efficient green dye for DSSC applications.[5]

* Corresponding authors. E-mail: cyyeh@dragon.nchu.edu.tw (C.-Y.Y.), diau@mail.nctu.edu.tw (E.W.-G.D.).
† National Chiao Tung University.
‡ National Chung Hsing University.

CHART 1: Molecular Structures of Three Zinc Porphyrin Sensitizers

The effect of aggregation on the TiO_2 surface is an important issue in further improving the cell performance of porphyrin-based DSSCs.[4−6] Aggregates do not contribute to photocurrent generation in devices made of tetrachelate porphyrin chromophores,[4c] and some push−pull porphyrins likewise suffer from dye aggregation.[5] To suppress dye aggregation on the TiO_2 surface, a remedy is to add a coadsorbate into the dye solution when fabricating sensitized TiO_2 films into devices. The most popular coadsorbate is chenodeoxycholic acid (CDCA),[4a,5] but other coadsorbates with either long alkyl chains (e.g., hexadecylmalonic acid or HDMA)[7] or bulky groups [e.g., dineohexyl bis(3,3-dimethylbutyl)phosphinic acid, or DINHOP][8] have also been reported. We report here results of our systematic characterizations of three zinc porphyrin sensitizers, **YD0**−**YD2** (Chart 1), coadsorbed with CDCA at three ratios on TiO_2 films with thicknesses of 5−10 μm with and without an added scattering layer with a thickness of ∼4 μm. Without a diarylamino group, **YD0** served as a reference for comparison with **YD1** and **YD2**. The diarylamino motif has been commonly applied in the preparation of push−pull organic dyes for HOMO−LUMO tuning.[9] **YD2** was modified from **YD1** in that

Control of Dye Aggregation and Electron Injection

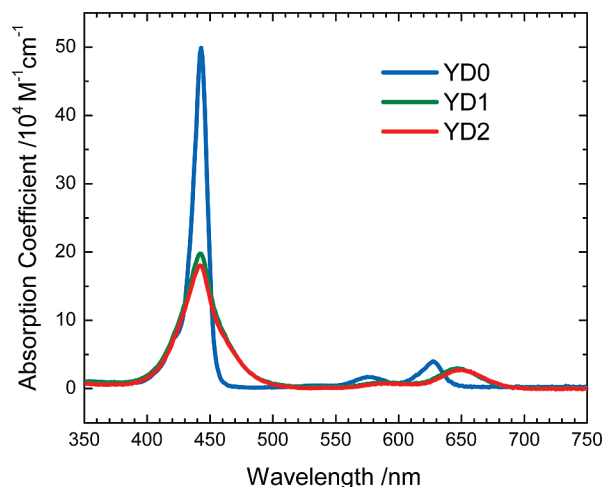*J. Phys. Chem. C, Vol. 113, No. 49, 2009* **20991**

Figure 1. Calibrated absorption spectra of **YD0**−**YD2** in ethanol.

the two *tert*-butyl groups in the diarylamino substituent were replaced with two long alkyl chains to improve its thermal and photochemical stability in a device.[10] This design mimics the strategy applied in an amphiphilic ruthenium polypyridyl sensitizer (**Z907**) that has shown excellent stability toward water-induced desorption under both thermal stress and light-soaking conditions.[11] The cell performances of **YD0** and **YD1** improved upon addition of CDCA at a dye/CDCA ratio of 1:2, whereas that of **YD2** decreased in the presence of CDCA. With femtosecond fluorescence up-conversion applied to both porphyrin-sensitized TiO$_2$ and Al$_2$O$_3$ films, we estimated the electron-injection yield (Φ_{inj}) for **YD0**−**YD2** and rationalized the discrepancy between **YD1** and **YD2**.

2. Results and Discussion

The syntheses of **YD0** and **YD1** are described elsewhere,[5] and that of **YD2** is available in the Supporting Information. Figure 1 shows absorption spectra of **YD0**−**YD2** in ethanol solution. Because of the electronic coupling between the aromatic substituent and the porphyrin ring, the Soret bands of **YD1** and **YD2** are broader and the Q bands of **YD1** and **YD2** are significantly shifted toward longer wavelengths compared to **YD0**. The absorption spectra of **YD1** and **YD2** are similar, apart from a slightly red-shifted shoulder of the Q band of **YD2**. The spectral features of **YD1** and **YD2** with broad Soret band and red-shifted Q bands serve to increase the harvesting of solar energy in a DSSC device, as explained in the following section.

2.1. Photovoltaic Properties of YD0−YD2 Coadsorbed with CDCA at Varying Ratios. These three porphyrins were sensitized on TiO$_2$ films with thicknesses of $L \approx 5$ μm and fabricated into DSSC devices to characterize their photovoltaic performance (Supporting Information). The photovoltaic measurements were performed with five identical working electrodes for each porphyrin (**YD0**−**YD2**) coadsorbed with CDCA at varying molar ratios under the same experimental conditions. The raw data for each current−voltage (J−V) measurement are summarized in Tables S1−S4 (Supporting Information) for **YD0**−**YD2** and **N719**, respectively; the corresponding averaged photovoltaic parameters are summarized in Table 1. Figure 2a−c shows typical J−V curves (working electrode a in Tables S1−S3 in the Supporting Information) of the porphyrin-based DSSC devices for **YD0**−**YD2**, respectively, with CDCA at varying molar ratios as indicated. Our results demonstrate two important points: the efficiencies of power conversion of **YD1** and **YD2** are significantly greater than those of **YD0**, reflecting the values

of the short-circuit photocurrent density (J_{SC}), and the addition of CDCA improved both the open-circuit voltage (V_{OC}) and the filling factor (FF) for all sensitizers. V_{OC} and FF in the presence of CDCA increase through suppression of dye aggregation[4a,5] to increase the injected electrons and modification of the TiO$_2$ electrode surface to increase electron interception.[3b] J_{SC} has a maximum value at a dye/CDCA ratio of 1:2 for **YD0** and **YD1**, in contrast with a maximum of J_{SC} in the absence of CDCA for **YD2**. The loading of dye (Table 1) systematically decreased with decreasing ratio of dye to CDCA for all three sensitizers; this trend is consistent with the variation of J_{SC} in **YD2**. The presence of CDCA thus failed to improve the cell performance of **YD2**, unlike for **YD0**, **YD1**, and other porphyrin sensitizers. For TiO$_2$ films with a thickness of ∼5 μm, the performance of the **YD2** device in the absence of CDCA attained an efficiency of $\eta = 5.7\%$, slightly greater than that of **N719** ($\eta = 5.5\%$) through the significantly greater J_{SC} of the former (11.0 vs 9.3 mA cm^{-2}).

Figure 3a−c shows spectra for the incident photon to current conversion efficiency (IPCE) of the same DSSC devices whose J−V characteristics appear in Figure 2a−c; the dashed curves represent the corresponding light-harvesting efficiencies (LHE) obtained from absorption spectra of the sensitized TiO$_2$ films. Integrating the IPCE over the AM 1.5G solar spectrum yields a calculated J_{SC} value similar to the collected value for all devices under investigation (Supporting Information Figure S1), thus validating the J−V results shown in Figure 2. The IPCE spectra of **YD0**−**YD2** mimic the corresponding LHE spectra in the range of 400−700 nm. We deduced two features from our IPCE results to account for the cell performances of **YD1** and **YD2** being superior to that of **YD0**. First, the IPCE spectra of **YD1** and **YD2** exhibit Soret and Q bands that are broadened and red-shifted relative to those of **YD0**, improving the light harvesting of the former. Second, the gaps between the LHE and IPCE spectra of **YD1** and **YD2** (20%) are smaller than that of **YD0** (∼30%), thereby increasing the capabilities of electron injection and charge collection for the former. As a result, the J_{SC} values of **YD1** and **YD2** are significantly greater than that of **YD0**. The presence of CDCA decreases the LHE for all porphyrins, but the IPCE spectra of **YD0** and **YD1** differ from that of **YD2**; the IPCE values are greatest for **YD0** and **YD1** for a dye/CDCA ratio of 1:2, whereas the IPCE spectrum of **YD2** varies little with dye/CDCA ratio. The IPCE results shown in Figure 3 are thus consistent with the J−V results shown in Figure 2.

2.2. Enduring Charge-Separation States of YD1 and YD2 on TiO$_2$ Films. The absorption (or LHE) spectra of the **YD1**/TiO$_2$ and **YD2**/TiO$_2$ films feature an additional band at about ∼800 nm, which **YD0** lacks. As the IPCE spectra of **YD1** and **YD2** show no signal near ∼800 nm, this 800-nm absorption band makes no contribution to photocurrent generation. In our work on the spectroelectrochemistry of **YD1**, two characteristic bands at ∼800 and ∼1350 nm were unambiguously observed for the oxidized species of **YD1**.[5] Such a spectral feature for the **YD1**/TiO$_2$ and **YD2**/TiO$_2$ films thus indicates the formation of the dye cationic species. To confirm this deduction, we performed additional experiments in three steps and observed the following results (Figure 4): (i) the 800- and 1350-nm bands were absent when we initially prepared a **YD1**/TiO$_2$ film under dark conditions, (ii) the two characteristic absorption bands appeared after the film was exposed to a lamp (100 mW cm^{-2}) for 1 min, and (iii) this spectral feature persisted until the film was further rinsed with a ferrocene/*tert*-butanol solution that eliminated the cationic spectral feature because **YD1**$^+$ became

TABLE 1: Photovoltaic Parameters of DSSCs with TiO$_2$ Films ($L \approx 5$ μm) Sensitized with YD0−YD2 and N719 Coadsorbed with Varying CDCA Ratios under Simulated AM-1.5 Illumination (Power = 100 mW cm^{-2}) and an Active Area of 0.16 cm^2 [a]

dye	dye/CDCA ratio	dye loading (nmol cm^{-2})	J_{SC} (mA cm^{-2})	V_{OC} (V)	FF	η (%)
YD0	1:0	50	6.46 ± 0.15	0.693 ± 0.004	0.727 ± 0.015	3.25 ± 0.09
	1:2	40	7.43 ± 0.52	0.707 ± 0.009	0.722 ± 0.058	3.79 ± 0.06
	1:10	35	6.30 ± 0.14	0.699 ± 0.009	0.735 ± 0.010	3.24 ± 0.03
YD1	1:0	59	9.02 ± 0.26	0.711 ± 0.008	0.668 ± 0.007	4.28 ± 0.11
	1:2	50	10.12 ± 0.56	0.720 ± 0.005	0.726 ± 0.011	5.29 ± 0.23
	1:10	46	9.05 ± 0.54	0.720 ± 0.007	0.717 ± 0.031	4.67 ± 0.09
YD2	1:0	72	11.00 ± 0.44	0.729 ± 0.004	0.710 ± 0.010	5.69 ± 0.15
	1:2	67	10.51 ± 0.25	0.728 ± 0.008	0.727 ± 0.011	5.56 ± 0.07
	1:10	58	10.16 ± 0.23	0.732 ± 0.006	0.731 ± 0.006	5.44 ± 0.12
N719	1:1	96	9.31 ± 0.20	0.792 ± 0.010	0.744 ± 0.013	5.48 ± 0.10

[a] Photovoltaic parameters are average values obtained from analysis of *J*−*V* curves of five identical working electrodes for each device fabricated and characterized under the same experimental conditions. The raw data of each *J*−*V* measurement are summarized in Tables S1−S4 (Supporting Information); the uncertainties represent two standard deviations of the measurements.
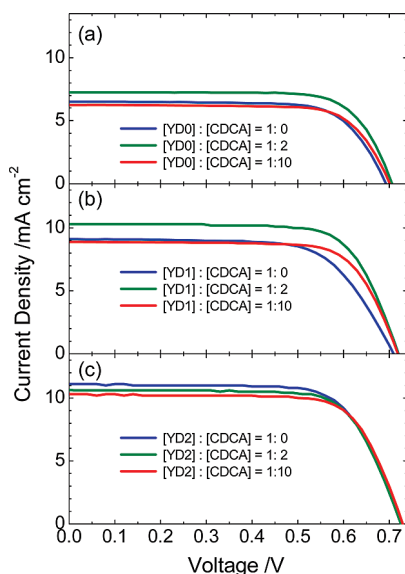

Figure 2. Current−voltage characteristics of DSSC devices (working electrode a in the Supporting Information) with sensitizers of (a) **YD0**, (b) **YD1**, and (c)**YD2** coadsorbed with CDCA in three ratios on a TiO$_2$ film with a thickness of ∼5 μm under illumination with simulated AM1.5G full sunlight (100 mW cm^{-2}) and an active area of 0.16 cm^2.
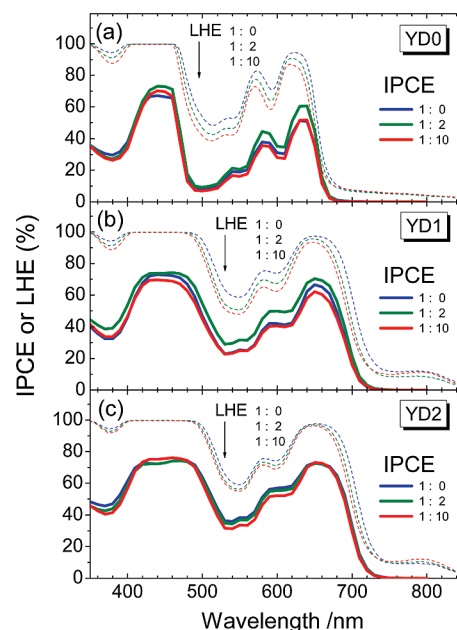

Figure 3. Corresponding action spectra for the efficiency of conversion of incident photons into current (IPCE) of the same DSSC devices as used for Figure 2. Dashed curves show the corresponding spectra of light-harvesting efficiency (LHE).

reduced to **YD1** by ferrocene; the same is true for **YD2**. We thereby confirmed that the appearance of the absorption band at 800 nm is due to the formation of an enduring cationic state of **YD1** or **YD2** on a TiO$_2$ film after photoinduced charge separation; this result implies the excellent character of charge separation in the **YD1**/TiO$_2$ and **YD2**/TiO$_2$ films with protracted charge recombination.

The observed retardation of charge recombination might reflect an optimal spatial separation between the amino moiety and the TiO$_2$ surface reported for a Ru-dye system.[12] For the porphyrin system, the period for charge recombination of a triarylamine-substituted porphyrin/TiO$_2$ film is 20 times that of a free-base porphyrin counterpart (80 vs 4 ms).[13] The smaller V_{OC} of porphyrin-sensitized solar cells reflects a decreased electron lifetime related to a rapid recombination of electrons with either dye cations or I$_3^-$ ions.[14] In our work, an enduring charge separation in porphyrin-sensitized TiO$_2$ films implies that the interception of conduction-band electrons is controlled solely by recombination of electrons with I$_3^-$. That the observed V_{OC} value in a **YD1**- or **YD2**-based DSSC is larger than those in **YD0**- and other porphyrin-based devices[4,14] is thus inferred to be due to the diminished recombination between I$_3^-$ and

conduction-band electrons, because I$_3^-$ might attach to the positively charged diarylamino moiety far from the TiO$_2$ surface.

2.3. Effect of CDCA on APCE Spectra. J_{SC} plays an important role in the efficiency of DSSC devices; the cell performance with varying CDCA ratio can thus be understood from the IPCE spectra in Figure 3. At each wavelength λ, the IPCE depends on the LHE, the quantum yield of electron injection (Φ_{inj}), and the efficiency of charge collection at the counter electrode (η_c) according to the expression[1b,15]

$$\text{IPCE}(\lambda) = \text{LHE}(\lambda)\Phi_{inj}\eta_c \quad (1)$$

Because LHE(λ) reflects the native absorption ability of a dye to capture the solar energy at wavelength λ, it is helpful to understand the electron-transport kinetics by expressing the absorbed photon to current conversion efficiency (APCE) according to[15]

$$\text{APCE} = \text{IPCE}(\lambda)/\text{LHE}(\lambda) = \Phi_{inj}\eta_c \quad (2)$$

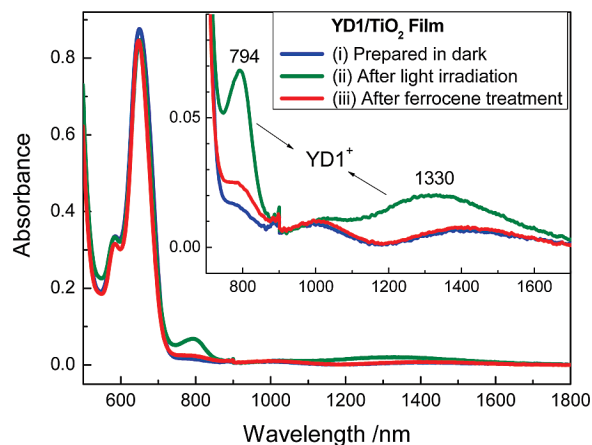Control of Dye Aggregation and Electron Injection

J. Phys. Chem. C, Vol. 113, No. 49, 2009 **20993**

Figure 4. Absorption spectra of a **YD1**/TiO$_2$ film ($L \approx 5~\mu m$) under consecutive processing. The film was (i) prepared initially in a dark environment, (ii) then irradiated with simulated sunlight (100 mW cm^{-2}) for 1 min, and (iii) finally rinsed with drops of a ferrocene/*tert*-butanol solution. The inset shows the corresponding enlarged spectra.
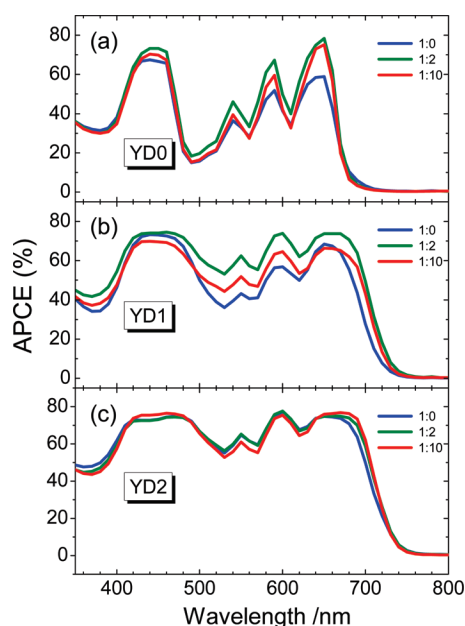

Figure 5. Spectra for the efficiency of conversion of absorbed photons to current (APCE) transformed from the corresponding IPCE and LHE spectra according to eq 2.

Figure 5a–c displays APCE spectra for **YD0–YD2**, respectively. The APCE values depend strongly on λ for **YD0**, but are less sensitive to λ in the visible region for **YD1** and **YD2**; the effect of CDCA on APCE is more pronounced for **YD1**, whereas the presence of CDCA has almost no influence on APCE for **YD2**. As APCE involves two parameters, namely, Φ_{inj} and η_c, the factor affecting the photovoltaic performances of these devices is understandable if one parameter can be well characterized. To estimate Φ_{inj} for the corresponding devices, we therefore measured femtosecond fluorescence up-conversion for TiO$_2$ films with thicknesses of 5 μm sensitized with **YD0–YD2** with CDCA added at various ratios.

2.4. Femtosecond Fluorescence Decays of YD0–YD2 on TiO$_2$ and Al$_2$O$_3$ Films. To investigate the dynamics of interfacial electron injection in porphyrin-sensitized TiO$_2$ films, we measured femtosecond fluorescence decays with porphyrin-sensitized Al$_2$O$_3$ films serving as references. The nanocrystalline TiO$_2$ films were prepared by the same method as was used for photovoltaic measurements; the preparation of nanocrystalline

Al$_2$O$_3$ films of the same thickness ($L \approx 5~\mu m$) is described in Supporting Information. To ensure that the amounts of dye loading on the two films are similar, we controlled the absorbances of the porphyrins on TiO$_2$ and Al$_2$O$_3$ films to be equal; the corresponding absorption spectra are shown in Figure S2 (Supporting Information).

Parts a–c of Figure 6 show normalized steady-state emission spectra of TiO$_2$ films of **YD0–YD2**, respectively; parts d–f of Figure 6 show the normalized steady-state emission spectra of Al$_2$O$_3$ films of **YD0–YD2**, respectively. These results indicate three important features: (i) the thin-film spectra exhibit a broad red-shifted spectral feature relative to their solution spectra, indicating the significance of dye aggregation on the surface of semiconductors; (ii) the emission spectra of **YD1** on Al$_2$O$_3$ films are shifted toward the solution spectra upon addition of CDCA at various ratios, but the spectral shifts of **YD2** are insensitive to the presence of CDCA on either film; and (iii) the relative intensities of the emissions of the Al$_2$O$_3$ films are significantly greater than those of the corresponding TiO$_2$ films, indicating the occurrence of electron injection from the excited state of a porphyrin to the conduction band of TiO$_2$. Thus time-resolved information is crucial for understanding the details of electron injection occurring at the dye/TiO$_2$ interface and the intermolecular energy transfer of the dye molecules on the surface of the films.

With excitation of thin-film samples at 430 nm,[4h,6b] the emissions at the maximum intensity were optically gated with the fundamental pulse (860 nm) to yield the emission decays of **YD0–YD2** on TiO$_2$ films as shown in Figure 7a–c, respectively, and on Al$_2$O$_3$ films as shown in Figure 7d–f, respectively. These transients show decays much more rapid for **YD1** and **YD2** than for **YD0** and for TiO$_2$ films than for Al$_2$O$_3$ films, but slower when more CDCA is added; such a feature was not obvious for **YD2**. The temporal profiles of all thin-film samples are characterized with a multiexponential decay; the corresponding time coefficients were obtained on analyzing the data with a parallel kinetic model

$$A \xrightarrow{\tau_1} B$$

$$A' \xrightarrow{\tau_2} B'$$

$$A'' \xrightarrow{\tau_3} B''$$
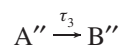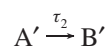
In this model, we assume that A, A′, and A″ are excited-state species of the dye molecule at separate sites of the surface of the semiconductor undergoing nonradiative relaxations through distinct channels to the corresponding dark states, B, B′, and B″; τ_1, τ_2, and τ_3 are their corresponding first-order decay coefficients. For Al$_2$O$_3$ films, three decay components are required to fit the fluorescence transients; for TiO$_2$ films, only two components are sufficient for the fits. The detailed deconvoluted components of the fitted curves are shown in Figures S3–S5 (Supporting Information) for **YD0–YD2**, respectively.

The relaxations of porphyrins on TiO$_2$ and Al$_2$O$_3$ films exhibit such a multiple-exponential feature because of the surface inhomogeneity of the semiconductors. To resolve the kinetics resulting from energy transfer and electron injection, we averaged the time coefficients according to the amplitude-averaged decay periods,[16] i.e., $\tau_{TiO_2} = \tau_1 A_1 + \tau_2 A_2$ and $\tau_{Al_2O_3} = \tau_1 A_1 + \tau_2 A_2 + \tau_3 A_3$; A_i represents the relative amplitudes, subject
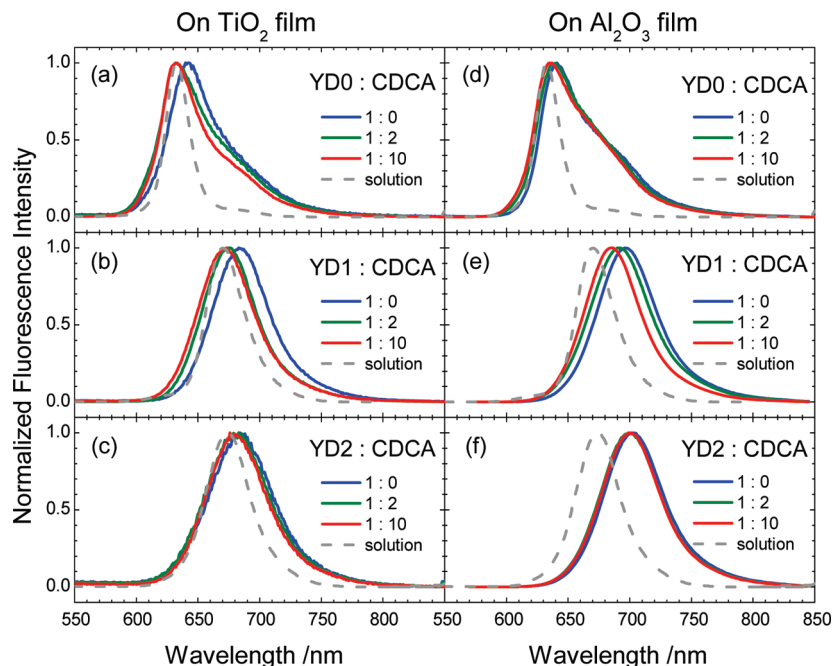
Figure 6. Steady-state fluorescence spectra of samples ($L \approx 5$ μm) of the same type as used for measurements of femtosecond fluorescence up-conversion: **YD0−YD2** with varying CDCA ratios coadsorbed on (a−c) TiO$_2$ films and (d−f) Al$_2$O$_3$ films.
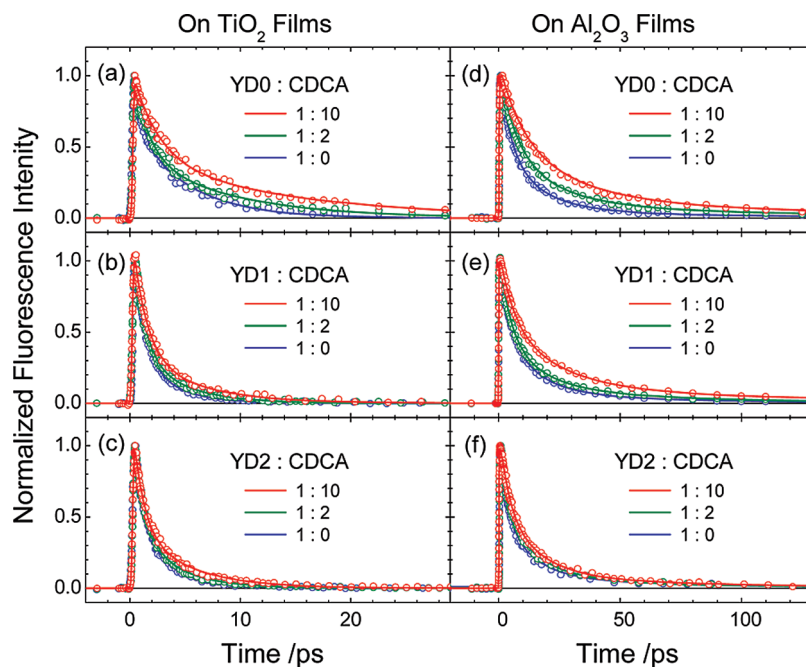

Figure 7. Femtosecond fluorescence decays of samples ($L \approx 5$ μm) obtained from measurements of femtosecond fluorescence up-conversion: transients of **YD0−YD2** with varying CDCA ratios coadsorbed on (a−c) TiO$_2$ films and (d−f) Al$_2$O$_3$ films.

to the condition $\sum_i A_i = 1.0$. The corresponding rate coefficients were determined according to $k_{TiO_2} = \tau_{TiO_2}^{-1}$ and $k_{Al_2O_3} = \tau_{Al_2O_3}^{-1}$. The emission decays of the porphyrin/Al$_2$O$_3$ films reflect only the intermolecular energy transfer because of aggregation of the dye on the Al$_2$O$_3$ surface, but the emission decays of the porphyrin/TiO$_2$ films not only contain the aggregate-induced energy transfer but also reflect the rapid electron injection from the excited state of the dye into the conduction band of TiO$_2$. If we assume that the extents of dye aggregation on the two films are similar, based on the same amounts of dye molecules adsorbed on the films with similar nanostructural morphologies, the rate coefficient for electron injection from an excited porphyrin into the TiO$_2$ surface is determined by $k_{inj} \approx k_{TiO_2}$

$- k_{Al_2O_3}$. These amplitude-averaged kinetic parameters for **YD0−YD2** with varying CDCA ratios sensitized on the TiO$_2$ and Al$_2$O$_3$ films are summarized in Table 2.

The rate coefficients ($k_{Al_2O_3}$) for aggregate-induced energy transfer decrease in the order **YD2 > YD1 > YD0** in the absence of CDCA, but the decrease of the rate coefficients in the presence of CDCA is in the oppositely order; e.g., for a dye/CDCA ratio varying from 1:0 to 1:10, the values of $k_{Al_2O_3}$ for **YD0** decreased by two-thirds, but those of **YD2** decreased by only ∼20%. The large $k_{Al_2O_3}$ values and great spectral shifts of films vs solution (Figure 6f) of **YD2** indicate the occurrence of dye aggregation to some extent on semiconductor films, but the small variation of $k_{Al_2O_3}$ and the small spectral shifts with

Control of Dye Aggregation and Electron Injection

J. Phys. Chem. C, Vol. 113, No. 49, 2009 **20995**

TABLE 2: Kinetic Parameters of TiO$_2$ and Al$_2$O$_3$ Films ($L \approx 5$ μm) Sensitized with YD0−YD2 Coadsorbed with Varying CDCA Ratios Obtained from Analysis of Femtosecond Fluorescence Decays Shown in Figure 7[a]

dye	dye/CDCA ratio	τ_{TiO_2} (ps)	$\tau_{Al_2O_3}$ (ps)	k_{TiO_2} (10^{11}s^{-1})	$k_{Al_2O_3}$ (10^{11}s^{-1})	k_{inj} (10^{11}s^{-1})	Φ_{inj} (%)
YD0	1:0	2.55 ± 0.15	13.5 ± 2.7	3.92 ± 0.23	0.74 ± 0.14	3.18 ± 0.27	0.81 ± 0.08
	1:2	4.52 ± 0.22	23.5 ± 4.7	2.21 ± 0.11	0.43 ± 0.09	1.78 ± 0.14	0.81 ± 0.08
	1:10	6.67 ± 0.35	41.4 ± 5.5	1.50 ± 0.08	0.24 ± 0.03	1.26 ± 0.09	0.84 ± 0.07
YD1	1:0	1.60 ± 0.08	11.8 ± 1.7	6.25 ± 0.31	0.85 ± 0.12	5.40 ± 0.33	0.86 ± 0.07
	1:2	1.96 ± 0.09	14.8 ± 2.8	5.10 ± 0.23	0.68 ± 0.12	4.42 ± 0.26	0.87 ± 0.06
	1:10	2.57 ± 0.12	23.4 ± 3.2	3.89 ± 0.18	0.43 ± 0.06	3.46 ± 0.19	0.89 ± 0.06
YD2	1:0	1.71 ± 0.10	10.5 ± 1.6	5.85 ± 0.34	0.95 ± 0.14	4.90 ± 0.37	0.84 ± 0.08
	1:2	2.05 ± 0.09	12.1 ± 2.2	4.88 ± 0.21	0.83 ± 0.15	4.05 ± 0.26	0.83 ± 0.06
	1:10	2.41 ± 0.16	13.5 ± 2.5	4.15 ± 0.28	0.74 ± 0.14	3.41 ± 0.31	0.82 ± 0.09

[a] Average time coefficients obtained from raw data shown in Figures S3−S5 (Supporting Information), using the amplitude-averaged decay times. The uncertainties represent two standard deviations obtained from nonlinear curve fitting and subsequent data analysis.

increasing amount of CDCA imply that the coadsorbate cannot effectively suppress porphyrin aggregation for **YD2**. The porphyrins hence seemed to form aggregate clusters on semiconductor films. When CDCA is added for **YD0** and **YD1**, the coadsorbate might enter the interspace of each cluster so that $k_{Al_2O_3}$ decreases substantially; for **YD2**, CDCA might enter the interspace of the aggregate clusters less effectively, probably because of the hindrance of the two hydrophobic hexyl chains, so that $k_{Al_2O_3}$ decreases only slightly.

The rate coefficients (k_{inj}) for electron injection of **YD1** and **YD2** are significantly larger than that of **YD0**, reflecting the superior electron-donating ability of the former with the diarylamino substituents. The values of k_{inj} also depend on the dye/CDCA ratio for all three porphyrins: the more CDCA added, the smaller the value of k_{inj}. For an increas in the dye/CDCA ratio from 1:0 to 1:10, k_{inj} decreased in the order **YD0** > **YD1** ≈ **YD2**. Porphyrin aggregation on TiO$_2$ surfaces thus not only accelerates the rate of intermolecular energy transfer, represented by $k_{Al_2O_3}$, but also increases, to some extent, the rate of interfacial electron injection represented by k_{inj}, so that the yields of electron injection are balanced by these two important factors.

Electron injection from an electronically excited state of a porphyrin into the conduction band of TiO$_2$ competes with other radiative or nonradiative relaxation channels. The quantum yield, Φ_{inj}, for electron injection, which defines the fraction of photons absorbed by the porphyrin that become converted into electrons in the conduction band of TiO$_2$, is formulated as

$$\Phi_{inj} = \frac{k_{inj}}{k_{inj} + k_{agg} + k_{nr} + k_r} = \frac{k_{inj}}{k_{TiO_2}} \approx$$

$$(\tau_{TiO_2}^{-1} - \tau_{Al_2O_3}^{-1})\tau_{TiO_2} = 1 - \frac{\tau_{TiO_2}}{\tau_{Al_2O_3}} \quad (3)$$

where k_{agg} represents the nonradiative rate coefficient for aggregate-induced energy transfer so that it is equal to $k_{Al_2O_3}$. k_r and k_{nr} represent the rate coefficients for radiative and other nonradiative (e.g., intersystem crossing) processes, respectively. The values of Φ_{inj} calculated according to eq 3 are summarized in the rightmost column of Table 2. For both **YD0** and **YD1**, Φ_{inj} increased slightly with increasing amount of CDCA because the rate of energy transfer decreased more than the rate of electron injection, but Φ_{inj} decreased slightly with increasing amount of CDCA for **YD2** because the variation of the rate coefficients was in the other direction. Even though the variations are within the experimental uncertainties, our results are consistent with the presence of CDCA not improving the photovoltaic performance for **YD2** as it did for **YD0** and **YD1**.

Because of similar APCE values for **YD1** (1:2) and **YD2** (1:0), Φ_{inj} for **YD1** being larger than that for **YD2** implies that the efficiency of charge collection of **YD2** is superior to that of **YD1** through an advantage of two long hydrophobic alkyl chains in the diarylamino group of **YD2**.

2.5. Optimization of Cell Performance for YD0−YD2 on Thicker TiO$_2$ Films. At the optimal conditions for the **YD0**−**YD2** devices, we performed photovoltaic measurements for the three porphyrins sensitized on TiO$_2$ films with thicknesses of ∼10 μm without and with an added scattering layer with a thickness of ∼4 μm. We similarly performed photovoltaic measurements of **YD0**−**YD2** and **N719** with three identical working electrodes under the same experimental conditions. The raw data for each current−voltage (J−V) measurement are summarized in Tables S5 and S6 (Supporting Information) for TiO$_2$ films without and with the scattering layer, respectively; the corresponding average photovoltaic parameters are summarized in Table 3. Figure 8a,b shows typical J−V curves (working electrode a in Tables S5 and S6, Supporting Information) for TiO$_2$ films without and with the scattering layer, respectively; the corresponding IPCE spectra appear in Figure 8c,d. Integrating the IPCE over the AM 1.5G solar spectra again yielded calculated J_{SC} values that matched perfectly with the collected values for all devices under investigation (see Figure S6 in the Supporting Information).

Our results indicate that both **YD1** (1:2) and **YD2** (1:0) exhibit remarkable performances relative to **N719** (1:1) without a scattering layer; the performance of **YD0** (1:2) is significantly less than that of the others. **YD2** performs even better than **YD1** because the larger J_{SC} value results from the more intense and broader IPCE spectrum shown in Figure 8c. The J_{SC} values of these two promising porphyrin-based devices, **YD1** and **YD2**, are greater than that of the **N719** device. Even though the V_{OC} and FF values for the former are smaller than those for the latter, the net effects of these variations make the overall efficiencies of power conversion of the **YD1** and **YD2** devices superior to that of the **N719** device. **YD1** ($\eta = 6.4\%$) and **YD2** ($\eta = 6.6\%$) are thus two green sensitizers that are remarkable for their outstanding cell performances relative to that of **N719** ($\eta = 6.3\%$) without an added scattering layer for green-light-penetrable DSSC applications.

When TiO$_2$ films with thicknesses of ∼10 μm were covered with a scattering layer with a thickness of ∼4 μm, the cell performance of **N719** was improved significantly to $\eta = 7.3\%$, whereas the performances of the porphyrin dyes increased only slightly, to $\eta = 6.5\%$ and 6.8% for **YD1** and **YD2**, respectively. The IPCE spectra of **YD1** and **YD2** exhibit a large gap between the Soret and the Q bands without a scattering layer (Figure 8c), but this gap is decreased for the TiO$_2$ films with a scattering

TABLE 3: Photovoltaic Parameters of DSSCs with TiO$_2$ Films [$L \approx 10$ or $(10 + 4)$ μm] Sensitized with YD0−YD2 and N719 Coadsorbed with Varying CDCA Ratios under Simulated AM-1.5 Illumination (Power = 100 mW cm^{-2}) and an Active Area of 0.16 cm^2 [a]

dye (dye/CDCA)	L (μm)	J_{SC} (mA cm^{-2})	V_{OC} (V)	FF	η (%)
YD0 (1:2)	$\sim$10	8.11 ± 0.04	0.700 ± 0.009	0.741 ± 0.008	4.21 ± 0.08
	$\sim$(10 + 4)	8.63 ± 0.20	0.706 ± 0.002	0.744 ± 0.006	4.53 ± 0.06
YD1 (1:2)	$\sim$10	12.80 ± 0.28	0.710 ± 0.003	0.707 ± 0.008	6.42 ± 0.05
	$\sim$(10 + 4)	13.05 ± 0.45	0.712 ± 0.003	0.703 ± 0.018	6.54 ± 0.16
YD2 (1:0)	$\sim$10	13.43 ± 0.24	0.711 ± 0.004	0.694 ± 0.014	6.62 ± 0.12
	$\sim$(10 + 4)	13.68 ± 0.57	0.711 ± 0.003	0.695 ± 0.023	6.76 ± 0.13
N719 (1:1)	$\sim$10	11.64 ± 0.87	0.760 ± 0.010	0.712 ± 0.040	6.30 ± 0.11
	$\sim$(10 + 4)	13.83 ± 0.36	0.760 ± 0.008	0.698 ± 0.010	7.33 ± 0.08

[a] The photovoltaic parameters are averaged values obtained from analysis of the $J-V$ curves of three identical working electrodes for each device fabricated and characterized under the same experimental conditions; the raw data of each $J-V$ measurement are summarized in Tables S5 and S6 (Supporting Information), for L /μm $\approx$ 10 and $\approx$ (10 + 4), respectively; the uncertainties represent two standard deviations of the measurements.
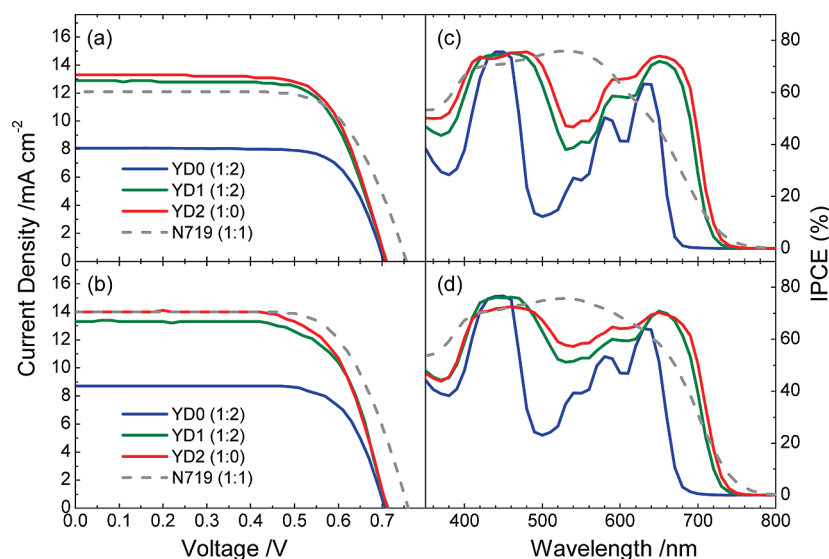

Figure 8. Optimal current−voltage characteristics of DSSC devices **YD0**−**YD2** (working electrode a in the Supporting Information) on TiO$_2$ films (thickness $\approx$ 10 μm) (a) without a scattering layer and (b) with a scattering layer (thickness $\approx$ 4 μm) under illumination of simulated AM1.5G full sunlight (100 mW cm^{-2}) and an active area 0.16 cm^2. (c,d) Corresponding IPCE action spectra. The gray dashed curves in all plots show the results for **N719** devices for comparison.

layer (Figure 8d). The shoulders of the efficiency spectra on the red side extended no further beyond the edge of the Q band in the presence of a scattering layer; for this reason, only a slight improvement in J_{SC} was found for the porphyrin-based DSSCs with a scattering layer. In contrast, the cell performance improved significantly for an **N719**-based DSSC with a scattering layer because of the effective scattering effect in the red shoulder of the efficiency spectrum.

3. Summary and Concluding Remarks

We report here photovoltaic performances and femtosecond fluorescence kinetics for three porphyrin sensitizers (**YD0**−**YD2**) coadsorbed with chenodeoxycholic acid (CDCA) at three molar ratios on nanocrystalline semiconductor films of TiO$_2$ and Al$_2$O$_3$. Our photovoltaic results revealed three important points summarized as follows: First, devices **YD1** and **YD2** made of porphyrins with electron-donating substituents outperform reference cell **YD0** because of the effective electronic coupling between the diarylamino group and the porphyrin core that makes the IPCE spectra of the former much broader and red-shifted compared to the latter. Second, the addition of CDCA improved the cell performances of **YD0** and **YD1** to attain the greatest efficiencies at a dye/CDCA ratio of 1:2, but the presence of CDCA had a negative effect for **YD2**. Third,

the efficiencies of power conversion of **YD1** and **YD2** are slightly greater than that of **N719** (6.4% and 6.6% vs 6.3%) without an added scattering layer on a TiO$_2$ film with a thickness of $\sim$10 μm, but when the 10-μm TiO$_2$ films were covered with a scattering layer with a thickness of $\sim$4 μm, the cell performance of **N719** significantly improved to η = 7.3%, whereas the performances of **YD1** and **YD2** increased only slightly, to η = 6.5% and 6.8%. The reason is that the shoulders of the IPCE spectra of **YD1** and **YD2** on the red side extended no further beyond the edge of the Q band, but such a scattering effect in the red shoulder significantly enhanced J_{SC} for device **N719** with a scattering layer.

The superlative cell performances of **YD1** and **YD2** are due to their large J_{SC} values, which arise from the uniformly large efficiency broadly covering the entire visible region of the solar spectrum. The diarylamino group attached at the meso position of the porphyrin core not only extends the absorption *spectrally* to a region of greater wavelength but also pushes the excited electrons *spatially* toward the TiO$_2$ film for an improved charge separation. Both **YD1** and **YD2** adsorbed on a TiO$_2$ surface exhibit a long-lived cationic spectral feature corresponding to the absorption bands at $\sim$800 and $\sim$1350 nm for their protracted charge recombination, whereas this spectral feature was absent when they were adsorbed on Al$_2$O$_3$ films or for **YD0** adsorbed

Control of Dye Aggregation and Electron Injection

J. Phys. Chem. C, Vol. 113, No. 49, 2009 **20997**

on both films. The existence of the enduring charge-separation state in the porphyrin-sensitized TiO_2 films implies that the interception of conduction-band electrons is controlled solely by recombination of the electrons with I_3^- in the electrolyte. That the cell performances of **YD1** and **YD2** are superior to that of **YD0** is thus due to the diminished recombination between I_3^- and conduction-band electrons, because I_3^- might attach to the positively charged diarylamino moiety far from the TiO_2 surface.

Because dye aggregation is an important issue for further improvement of the cell performance for porphyrin-based DSSC, we investigated the excited-state relaxation dynamics of **YD0**−**YD2** with **N719** at various ratios coadsorbed on TiO_2 or Al_2O_3 films (thickness ≈ 5 μm) using femtosecond fluorescence up-conversion. The order of rates of aggregate-induced energy transfer of porphyrins on Al_2O_3 films is **YD2** > **YD1** > **YD0** in the absence of CDCA, but the rate of energy transfer in the presence of CDCA decreased much less for **YD2** than for **YD0** and **YD1**. The rates of electron injection of **YD1** and **YD2** are significantly greater than those of **YD0**, confirming that the involvement of the diarylamino substitutes in **YD1** and **YD2** has a dynamic effect to push the electrons efficiently toward TiO_2. As the rates of electron injection for all three porphyrins decreased when more CDCA was added, porphyrin aggregation on TiO_2 surfaces not only accelerated the rate of intermolecular energy transfer but also increased the rate of interfacial electron injection so that the yields (Φ_{inj}) of electron injection were balanced by these two important factors. As a result, Φ_{inj} increased slightly with increasing amount of CDCA for both **YD0** and **YD1**, but the variation in Φ_{inj} was reversed for **YD2** because the rate of electron injection decreased more significantly than the rate of energy transfer for the latter. The femtosecond results thus explain why the presence of CDCA failed to improve the photovoltaic performance for **YD2** unlike for **YD0** and **YD1**. The presence of CDCA suppresses dye aggregation, decreases the amount of dye loading on the TiO_2 surface and diminishes electron injection from dye to TiO_2; the overall performance of a porphyrin-based DSSC is thus a subtle balance between these factors.

Supporting Information Available: Synthesis and characterization of **YD2**, electrode preparation and device fabrication, effect of dye loading, photovoltaic characterization, femtosecond fluorescence spectra, and supplementary tables (Tables S1−S6) and figures (Figures S1−S6). This material is available free of charge via the Internet at http://pubs.acs.org.

References and Notes

(1) (a) O'Regan, B.; Grätzel, M. *Nature* **1991**, *353*, 737. (b) Nazeeruddin, M. K.; Kay, A.; Rodicio, I.; Humphry-Baker, R.; Müller, E.; Liska, P.; Vlachopoulos, N.; Grätzel, M. *J. Am. Chem. Soc.* **1993**, *115*, 6382. (c) Grätzel, M. *Inorg. Chem.* **2005**, *44*, 6841.

(2) (a) Wang, Q.; Ito, S.; Grätzel, M.; Fabregat-Santiago, F.; Mora-Seró, I.; Bisquert, J.; Bessho, T.; Imai, H. *J. Phys. Chem. B* **2006**, *110*, 25210. (b) Gao, F.; Wang, Y.; Shi, D.; Zhang, J.; Wang, M.; Jing, X.; Humphry-Baker, R.; Wang, P.; Zakeeruddin, S. M.; Grätzel, M. *J. Am. Chem. Soc.* **2008**, *130*, 10720.

(3) (a) Robertson, N. *Angew. Chem., Int. Ed.* **2006**, *45*, 2338. (b) Hamann, T. W.; Jensen, R. A.; Martinson, A. B. F.; Ryswyk, H. V.; Hupp, J. T. *Energy Environ. Sci.* **2008**, *1*, 66. (c) Mishra, A.; Fischer, M. K. R.; Bäuerle, P. *Angew. Chem., Int. Ed.* **2009**, *48*, 2474. (d) Imahori, H.; Umeyama, T.; Ito, S. *Acc. Chem. Res.*, published online May 1, 2009, http://dx.doi.org/10.1021/ar900034t.

(4) (a) Wang, Q.; Campbell, W. M.; Bonfantani, E. E.; Jolley, K. W.; Officer, D. L.; Walsh, P. J.; Gordon, K.; Humphry-Baker, R.; Nazeeruddin, M. K.; Grätzel, M. *J. Phys. Chem. B* **2005**, *109*, 15397. (b) Campbell, W. M.; Jolley, K. W.; Wagner, P.; Wagner, K.; Walsh, P. J.; Gordon, K. C.; Schmidt-Mende, L.; Nazeeruddin, M. K.; Wang, Q.; Grätzel, M.; Officer, D. L. *J. Phys. Chem. C* **2007**, *111*, 11760. (c) Rochford, J.; Chu, D.; Hagfeldt, A.; Galoppini, E. *J. Am. Chem. Soc.* **2007**, *129*, 4655. (d) Eu, S.; Hayashi, S.; Umeyama, T.; Oguro, A.; Kawasaki, M.; Kadota, N.; Matano, Y.; Imahori, H. *J. Phys. Chem. C* **2007**, *111*, 3528. (e) Stromberg, J. R.; Marton, A.; Kee, H. L.; Kirmaier, C.; Diers, J. R.; Muthiah, C.; Taniguchi, M.; Lindsey, J. S.; Bocian, D. F.; Meyer, G. J.; Holten, D. *J. Phys. Chem. C* **2007**, *111*, 15464. (f) Hayashi, S.; Tanaka, M.; Hayashi, H.; Eu, S.; Umeyama, T.; Matano, Y.; Araki, Y.; Imahori, H. *J. Phys. Chem. C* **2008**, *112*, 15576. (g) Park, J. K.; Lee, H. R.; Chen, J.; Shinokubo, H.; Osuka, A.; Kim, D. *J. Phys. Chem. C* **2008**, *112*, 16691. (h) Lin, C.-Y.; Lo, C.-F.; Luo, L.; Lu, H.-P.; Hung, C.-S.; Diau, E. W.-G. *J. Phys. Chem. C* **2009**, *113*, 755. (i) de Tacconi, N. R.; Chanmanee, W.; Rajeshwar, K.; Rochford, J.; Galoppini, E. *J. Phys. Chem. C* **2009**, *113*, 2996.

(5) Lee, C.-W.; Lu, H.-P.; Lan, C.-M.; Huang, Y.-L.; Liang, Y.-R.; Yen, W.-N.; Liu, Y.-C.; Lin, Y.-S.; Diau, E. W.-G.; Yeh, C.-Y. *Chem.—Eur. J.* **2009**, *115*, 1403.

(6) (a) Galoppini, E. *Coord. Chem. Rev.* **2004**, *248*, 1283. (b) Luo, L.-Y.; Lo, C.-F.; Lin, C.-Y.; Chang, I.-J.; Diau, E. W.-G. *J. Phys. Chem. B* **2006**, *110*, 410. (c) Lo, C.-F.; Luo, L.; Diau, E. W.-G.; Chang, I.-J.; Lin, C.-Y. *Chem. Commun.* **2006**, 1430.

(7) Wang, P.; Zakeeruddin, S. M.; Comte, P.; Charvet, R.; Humphry-Baker, R.; Grätzel, M. *J. Phys. Chem. B* **2003**, *107*, 14336.

(8) Wang, M.; Li, X.; Lin, H.; Pechy, P.; Zakeeruddin, S. M.; Grätzel, M. *Dalton Trans.*, published online 2009, http://dx.doi.org/10.1039/b908673k.

(9) Lu, H.-P.; Mai, C.-L.; Tsia, C.-Y.; Hsu, S.-J.; Hsieh, C.-P.; Chiu, C.-L.; Yeh, C.-Y.; Diau, E. W.-G. *Phys. Chem. Chem. Phys.* **2009**, *11*, 10270.

(10) (a) Hagberg, D. P.; Marinado, T.; Karlsson, K. M.; Nonomura, K.; Qin, P.; Boschloo, G.; Brinck, T.; Hagfeldt, A.; Sun, L. *J. Org. Chem.* **2007**, *72*, 9550. (b) Hagberg, D. P.; Yum, J.-H.; Lee, H.; De Angelis, F.; Marinado, T.; Karlsson, K. M.; Humphry-Baker, R.; Sun, L.; Hagfeldt, A.; Grätzel, M.; Nazeeruddin, Md. K. *J. Am. Chem. Soc.* **2008**, *130*, 6259. (c) Ooyama, Y.; Harima, Y. *Eur. J. Org. Chem.* **2009**, *18*, 2903.

(11) (a) Zakeeruddin, S. M.; Nazeeruddin, Md. K.; Humphry-Baker, R.; Péchy, P.; Quagliotto, P.; Barolo, C.; Viscardi, G.; Grätzel, M. *Langmuir* **2002**, *18*, 952. (b) Wang, P.; Zakeeruddin, S. M.; Moser, J. E.; Nazeeruddin, Md. K.; Sekiguchi, T.; Grätzel, M. *Nat. Mater.* **2003**, *2*, 402.

(12) (a) Hirata, N.; Lagref, J.-J.; Palomares, E. J.; Durrant, J. R.; Nazeeruddin, M. K.; Grätzel, M. *Chem.—Eur. J.* **2004**, *10*, 595. (b) Haque, S. A.; Handa, S.; Peter, K.; Palomares, E.; Thelakkat, M.; Durrant, J. R. *Angew. Chem., Int. Ed.* **2005**, *44*, 5740.

(13) Clifford, J. N.; Yahioglu, G.; Milgrom, L. R.; Durrant, J. R. *Chem. Commun.* **2002**, 1260.

(14) Mozer, A. J.; Wagner, P.; Officer, D. L.; Wallace, G. G.; Campbell, W. M.; Miyashita, M.; Sunahara, K.; Mori, S. *Chem. Commun.* **2008**, 4741.

(15) Halmes, J.; Boschloo, G.; Hagfeldt, A.; Lund, P. *J. Phys. Chem. C* **2008**, *112*, 5623.

(16) Valeur, B. *Molecular Fluorescence: Principles and Applications*; Wiley-VCH: New York, 2002.